PHYSICAL REVIEW D **95,** 115014 (2017)

Two-Higgs-doublet model of type II confronted with the LHC run I and run II data

Lei Wang,[1] Feng Zhang,[2,*] and Xiao-Fang Han[1,†]

[1]*Department of Physics, Yantai University, Yantai 264005, People's Republic of China*
[2]*Basic Teaching Department, Dalian Institute of Science and Technology, Dalian 116052, People's Republic of China*

(Received 3 April 2017; published 13 June 2017)

We examine the parameter space of the two-Higgs-doublet model of type II after imposing the relevant theoretical and experimental constraints from the precision electroweak data, B-meson decays, and the LHC run I and run II data. We find that the searches for Higgs bosons via the $\tau^+\tau^-$, WW, ZZ, $\gamma\gamma$, hh, hZ, HZ, and AZ channels can give strong constraints on the CP-odd Higgs A and heavy CP-even Higgs H, and the parameter space excluded by each channel is respectively carved out in detail assuming that either m_A or m_H are fixed to 600 or 700 GeV in the scans. The surviving samples are discussed in two different regions. (i) In the standard model–like coupling region of the 125 GeV Higgs, m_A is allowed to be as low as 350 GeV, and a strong upper limit is imposed on $\tan\beta$. m_H is allowed to be as low as 200 GeV for the appropriate values of $\tan\beta$, $\sin(\beta-\alpha)$, and m_A, but is required to be larger than 300 GeV for $m_A = 700$ GeV. (ii) In the wrong-sign Yukawa coupling region of the 125 GeV Higgs, the $b\bar{b} \to A/H \to \tau^+\tau^-$ channel can impose the upper limits on $\tan\beta$ and $\sin(\beta-\alpha)$, and the $A \to hZ$ channel can give the lower limits on $\tan\beta$ and $\sin(\beta-\alpha)$. m_A and m_H are allowed to be as low as 60 and 200 GeV, respectively, but 320 GeV $< m_A <$ 500 GeV is excluded for $m_H = 700$ GeV.

DOI: 10.1103/PhysRevD.95.115014

I. INTRODUCTION

The ongoing analyses of ATLAS and CMS show that the properties of the newly discovered 125 GeV boson are well consistent with the standard model (SM) Higgs boson [1–3]. No excesses are observed in the searches for the additional exotic Higgs. ATLAS and CMS have given us plentiful limits on additional scalar states from its decay into various SM channels and some exotic decays at the LHC run I and run II.

The two-Higgs-doublet model (2HDM) [4] extends the SM simply by adding a second $SU(2)_L$ Higgs doublet, which has very rich Higgs phenomenology, including two neutral CP-even Higgs bosons h and H, one neutral pseudoscalar A, and two charged Higgs $H^\pm$. According to the different Yukawa couplings, there are four types of 2HDMs which forbid the tree-level flavor-changing neutral currents: the type I [5,6], type II [5,7], lepton-specific, and flipped models [8–11]. Since the Yukawa couplings of both the down-type quark and lepton can be enhanced by a factor of $\tan\beta$, the type II model can be given more stringent constraints than the other three models by the flavor observables and the LHC searches for additional Higgses. The allowed parameter space of the 2HDM has been examined in light of the ATLAS and CMS searches for extra Higgses at the LHC in the literature [12–31].

In this paper we examine the parameter space of the type II 2HDM considering the joint constraints from theory, precision electroweak data, flavor observables, the 125 GeV Higgs signal data, and searches for the additional Higgs at the LHC run I and run II. The signal data of the 125 GeV Higgs allow the SM-like Higgs of the 2HDM to have the wrong-sign Yukawa coupling and the SM-like coupling. In the two different coupling regions of the SM-like Higgs, we respectively carve out the parameter space allowed by the relevant theoretical and experimental constraints, and obtain some interesting conclusions. Recently, there have been some similar works [30,31]. Compared to Refs. [30,31], we include more LHC searches for the Higgs in our analysis and obtain stronger constraints on the model. For example, we find that the CMS search for $b\bar{b} \to A/H \to \tau^+\tau^-$ in Ref. [32] can give stringent constraints on $\tan\beta$ and m_A (m_H). However, the corresponding upper limits on the channel from Ref. [32] were not considered in Refs. [30,31]. In addition, in this paper we examine the dependences of $\tan\beta$ and $\sin(\beta-\alpha)$ on the Higgs mass in detail, which were not fully shown in Refs. [30,31].

Our work is organized as follows. In Sec. II we briefly introduce the 2HDM of type II. In Sec. III we perform numerical calculations. In Sec. IV we show the allowed parameter space after imposing the relevant theoretical and experimental constraints. Finally, we give our conclusion in Sec. V.

*Corresponding author.
fzhangdist@126.com
†Corresponding author.
xfhan@mail.itp.ac.cn

II. TWO-HIGGS-DOUBLET MODEL OF TYPE II

The general Higgs potential with a softly broken discrete Z_2 symmetry is written as [33]

$$\begin{aligned}\mathrm{V} = & m_{11}^2(\Phi_1^\dagger\Phi_1) + m_{22}^2(\Phi_2^\dagger\Phi_2) - [m_{12}^2(\Phi_1^\dagger\Phi_2 + \mathrm{H.c.})] \\ & + \frac{\lambda_1}{2}(\Phi_1^\dagger\Phi_1)^2 + \frac{\lambda_2}{2}(\Phi_2^\dagger\Phi_2)^2 + \lambda_3(\Phi_1^\dagger\Phi_1)(\Phi_2^\dagger\Phi_2) \\ & + \lambda_4(\Phi_1^\dagger\Phi_2)(\Phi_2^\dagger\Phi_1) + \left[\frac{\lambda_5}{2}(\Phi_1^\dagger\Phi_2)^2 + \mathrm{H.c.}\right]. \end{aligned} \tag{1}$$

We focus on the CP-conserving model in which all λ_i and m_{12}^2 are real. The two complex scalar doublets have the hypercharge $Y = 1$:

$$\begin{aligned}\Phi_1 &= \begin{pmatrix} \phi_1^+ \\ \frac{1}{\sqrt{2}}(v_1 + \phi_1^0 + ia_1) \end{pmatrix}, \\ \Phi_2 &= \begin{pmatrix} \phi_2^+ \\ \frac{1}{\sqrt{2}}(v_2 + \phi_2^0 + ia_2) \end{pmatrix}, \end{aligned} \tag{2}$$

where v_1 and v_2 are the electroweak vacuum expectation values (VEVs) with $v^2 = v_1^2 + v_2^2 = (246\ \mathrm{GeV})^2$, and the ratio of the two VEVs is defined as $\tan\beta = v_2/v_1$. After spontaneous electroweak symmetry breaking, there are five mass eigenstates: two neutral CP-even states h and H, one neutral pseudoscalar A, and two charged scalars $H^\pm$.

The Yukawa interactions are written as

$$-\mathcal{L} = Y_{u2}\bar{Q}_L\tilde{\Phi}_2 u_R + Y_{d1}\bar{Q}_L\Phi_1 d_R + Y_{\ell 1}\bar{L}_L\Phi_1 e_R + \mathrm{H.c.}, \tag{3}$$

where $Q_L^T = (u_L, d_L)$, $L_L^T = (\nu_L, l_L)$, $\tilde{\Phi}_{1,2} = i\tau_2\Phi_{1,2}^*$, and Y_{u2}, Y_{d1}, and $Y_{\ell 1}$ are 3×3 matrices in family space.

The Yukawa couplings of the neutral Higgs bosons normalized to the SM are given as

$$\begin{aligned} & y_h^{f_i} = [\sin(\beta-\alpha) + \cos(\beta-\alpha)\kappa_f], \\ & y_H^{f_i} = [\cos(\beta-\alpha) - \sin(\beta-\alpha)\kappa_f], \\ & y_A^{f_i} = -i\kappa_f(\text{for u}), \qquad y_A^{f_i} = i\kappa_f(\text{for d}, \ell), \quad \text{with} \\ & \kappa_d = \kappa_\ell \equiv -\tan\beta, \qquad \kappa_u \equiv 1/\tan\beta. \end{aligned} \tag{4}$$

The Yukawa interactions of the charged Higgs are given as

$$\begin{aligned}\mathcal{L}_Y = & -\frac{\sqrt{2}}{v}H^+\{\bar{u}_i[\kappa_d(V_{CKM})_{ij}m_{dj}P_R \\ & - \kappa_u m_{ui}(V_{CKM})_{ij}P_L]d_j + \kappa_\ell\bar{\nu}m_\ell P_R\ell\} + \mathrm{H.c.}, \end{aligned} \tag{5}$$

where $i, j = 1, 2, 3$.

The neutral Higgs boson couplings with the gauge bosons normalized to the SM are given by

$$y_h^V = \sin(\beta-\alpha), \qquad y_H^V = \cos(\beta-\alpha), \tag{6}$$

where V denotes Z or W.

The properties of the observed 125 GeV Higgs are very close to the SM Higgs boson, which can give strong constraints on the sector of Higgs extensions. In the 2HDM, the SM-like Higgs is allowed to have the SM-like coupling and wrong-sign Yukawa coupling. For the former, the couplings of the 125 GeV Higgs are very close to the SM Higgs, which has a limit called the alignment limit. In the exact alignment limit [26,34], namely, $\cos(\beta-\alpha) = 0$, from Eqs. (4) and (6) we find that h has the same couplings to the fermions and gauge bosons as the SM, and the heavy CP-even Higgs (H) has no couplings to the gauge bosons.

In the wrong-sign Yukawa coupling region, at least one of the Yukawa couplings of the 125 GeV Higgs has the opposite sign to the coupling of the gauge boson. However, their absolute values should be close to the SM Higgs due to the constraints of 125 GeV Higgs signal data. Therefore, we can obtain

$$\begin{aligned} & y_h^{f_i} = -1 + \epsilon, \qquad y_h^V \simeq 1 - 0.5\cos^2(\beta-\alpha) \\ & \qquad \text{for } \sin(\beta-\alpha) > 0 \text{ and } \cos(\beta-\alpha) > 0, \\ & y_h^{f_i} = 1 - \epsilon, \qquad y_h^V \simeq -1 + 0.5\cos^2(\beta-\alpha) \\ & \qquad \text{for } \sin(\beta-\alpha) < 0 \text{ and } \cos(\beta-\alpha) > 0, \end{aligned} \tag{7}$$

where $|\epsilon|$ and $|\cos(\beta-\alpha)|$ are much smaller than 1. From Eq. (4), we can obtain

$$\begin{aligned} & \kappa_f = \frac{-2 + \varepsilon + 0.5\cos(\beta-\alpha)^2}{\cos(\beta-\alpha)} \ll -1 \\ & \qquad \text{for } \sin(\beta-\alpha) > 0 \text{ and } \cos(\beta-\alpha) > 0, \\ & \kappa_f = \frac{2 - \varepsilon - 0.5\cos(\beta-\alpha)^2}{\cos(\beta-\alpha)} \gg 1 \\ & \qquad \text{for } \sin(\beta-\alpha) < 0 \text{ and } \cos(\beta-\alpha) > 0. \end{aligned} \tag{8}$$

In the 2HDM of type II, $\tan\beta$ is required to be larger than 1 by the B-meson observables and R_b, leading to $\kappa_d < -1$, $\kappa_\ell < -1$, and $0 < \kappa_u < 1$ [see Eq. (4)]. Therefore, from Eq. (8) we obtain that in the 2HDM of type II there is no wrong-sign Yukawa coupling for the up-type quarks, and there may be wrong-sign Yukawa couplings for the down-type quark and lepton only for $\sin(\beta-\alpha) > 0$ and $\cos(\beta-\alpha) > 0$. For the same $\sin(\beta-\alpha)$, especially for $\sin(\beta-\alpha) \to 1$, $\tan\beta$ in the wrong-sign Yukawa coupling region is much larger than that of the SM-like coupling region. In other words, $\tan\beta$ has a lower bound in the wrong-sign Yukawa coupling region, and is allowed to approach 1 in the SM-like coupling region. In addition,

$\cos(\beta-\alpha)$ in the wrong-sign Yukawa coupling region is allowed to be much larger than that of the SM-like coupling region due to the presence of the -2 in the numerator of Eq. (8).

III. NUMERICAL CALCULATIONS

We take the light CP-even Higgs boson h as the SM-like Higgs, $m_h = 125$ GeV. The measurement of the branching fraction of $b \to s\gamma$ gives stringent constraints on the charged Higgs mass of the 2HDM of type II, $m_{H^\pm} > 570$ GeV [35].

In our calculation, we consider the following observables and constraints.

(1) Theoretical constraints and precision electroweak data: The program 2HDMC [36,37] is employed to implement the theoretical constraints from vacuum stability, unitarity, and coupling-constant perturbativity, as well as the constraints from the oblique parameters (S, T, U).

(2) The flavor observables and R_b: We consider the constraints of B-meson decays from $B \to X_s\gamma$, Δm_{B_s}, and Δm_{B_d}. SuperIso-3.4 [38] is used to calculate $B \to X_s\gamma$, and Δm_{B_s} and Δm_{B_d} are calculated using the formulas in Ref. [39]. In addition, we consider the constraints of bottom quarks produced in Z decays, R_b, which is calculated following the formulas in Refs. [40,41].

TABLE I. The upper limits at 95% C.L. on the production cross section times branching ratio of the processes considered in the H and A searches at the LHC run I and run II.

Channel	Experiment	Mass range (GeV)	Luminosity
$gg/b\bar{b} \to H/A \to \tau^+\tau^-$	ATLAS 8 TeV [49]	90–1000	19.5–20.3 fb^{-1}
$gg/b\bar{b} \to H/A \to \tau^+\tau^-$	CMS 8 TeV [32]	90–1000	19.7 fb^{-1}
$b\bar{b} \to H/A \to \tau^+\tau^-$	CMS 8 TeV [50]	20–80	19.7 fb^{-1}
$gg/b\bar{b} \to H/A \to \tau^+\tau^-$	ATLAS 13 TeV [51]	200–1200	13.3 fb^{-1}
$gg/b\bar{b} \to H/A \to \tau^+\tau^-$	CMS 13 TeV [52]	90–3200	12.9 fb^{-1}
$pp \to H/A \to \gamma\gamma$	ATLAS 13 TeV [53]	200–2400	15.4 fb^{-1}
$gg \to H/A \to \gamma\gamma$	CMS 8 + 13 TeV [54]	500–4000	12.9 fb^{-1}
$gg/VV \to H \to W^+W^-$	ATLAS 8 TeV [55]	300–1500	20.3 fb^{-1}
$gg/VV \to H \to W^+W^-(\ell\nu\ell\nu)$	ATLAS 13 TeV [56]	300–3000	13.2 fb^{-1}
$gg \to H \to W^+W^-(\ell\nu qq)$	ATLAS 13 TeV [57]	500–3000	13.2 fb^{-1}
$gg/VV \to H \to ZZ$	ATLAS 8 TeV [58]	160–1000	20.3 fb^{-1}
$gg \to H \to ZZ(\ell\ell\nu\nu)$	ATLAS 13 TeV [59]	300–1000	13.3 fb^{-1}
$gg \to H \to ZZ(\nu\nu qq)$	ATLAS 13 TeV [60]	300–3000	13.2 fb^{-1}
$gg/VV \to H \to ZZ(\ell\ell qq)$	ATLAS 13 TeV [60]	300–3000	13.2 fb^{-1}
$gg/VV \to H \to ZZ(4\ell)$	ATLAS 13 TeV [61]	200–3000	14.8 fb^{-1}
$gg \to H \to hh \to (\gamma\gamma)(b\bar{b})$	CMS 8 TeV [62]	250–1100	19.7 fb^{-1}
$gg \to H \to hh \to (b\bar{b})(b\bar{b})$	CMS 8 TeV [63]	270–1100	17.9 fb^{-1}
$gg \to H \to hh \to (b\bar{b})(\tau^+\tau^-)$	CMS 8 TeV [64]	260–350	19.7 fb^{-1}
$gg \to H \to hh \to (\gamma\gamma)(b\bar{b})$	ATLAS 13 TeV [65]	275–400	3.2 fb^{-1}
$gg \to H \to hh \to (\gamma\gamma)(b\bar{b})$	CMS 13 TeV [66]	250–900	2.7 fb^{-1}
$gg \to H \to hh \to b\bar{b}b\bar{b}$	ATLAS 13 TeV [48]	300–3000	13.3 fb^{-1}
$gg \to H \to hh \to b\bar{b}\tau^+\tau^-$	CMS 13 TeV [67]	250–900	12.9 fb^{-1}
$gg \to A \to hZ \to (\tau^+\tau^-)(\ell\ell)$	CMS 8 TeV [64]	220–350	19.7 fb^{-1}
$gg \to A \to hZ \to (b\bar{b})(\ell\ell)$	CMS 8 TeV [68]	225–600	19.7 fb^{-1}
$gg \to A \to hZ \to (\tau^+\tau^-)Z$	ATLAS 8 TeV [69]	220–1000	20.3 fb^{-1}
$gg \to A \to hZ \to (b\bar{b})Z$	ATLAS 8 TeV [69]	220–1000	20.3 fb^{-1}
$gg/b\bar{b} \to A \to hZ \to (b\bar{b})Z$	ATLAS 13 TeV [70]	200–2000	3.2 fb^{-1}
$gg \to A(H) \to H(A)Z \to (b\bar{b})(\ell\ell)$	CMS 8 TeV [71]	200–1000	19.8 fb^{-1}
$gg \to A(H) \to H(A)Z \to (\tau^+\tau^-)(\ell\ell)$	CMS 8 TeV [71]	200–1000	19.8 fb^{-1}

(3) The global fit to the 125 GeV Higgs signal data: We perform the χ^2 calculation for the signal strengths of the 125 GeV Higgs in $\mu_{ggF+tth}(Y)$ and $\mu_{VBF+Vh}(Y)$, with Y denoting the decay modes $\gamma\gamma$, ZZ, WW, $\tau^+\tau^-$, and $b\bar{b}$:

$$\chi^2(Y) = \begin{pmatrix} \mu_{ggH+ttH}(Y) - \hat{\mu}_{ggH+ttH}(Y) \\ \mu_{VBF+VH}(Y) - \hat{\mu}_{VBF+VH}(Y) \end{pmatrix}^T \times \begin{pmatrix} a_Y & b_Y \\ b_Y & c_Y \end{pmatrix} \times \begin{pmatrix} \mu_{ggH+ttH}(Y) - \hat{\mu}_{ggH+ttH}(Y) \\ \mu_{VBF+VH}(Y) - \hat{\mu}_{VBF+VH}(Y) \end{pmatrix}. \quad (9)$$

$\hat{\mu}_{ggH+ttH}(Y)$ and $\hat{\mu}_{VBF+VH}(Y)$ are the data best-fit values, and a_Y, b_Y, and c_Y are the parameters of the ellipse, which are given by the combined ATLAS and CMS experiments [3]. We pay particular attention to the surviving samples with $\chi^2 - \chi^2_{\rm min} \leq 6.18$, where $\chi^2_{\rm min}$ denotes the minimum of χ^2. These samples correspond to being within the 2σ range in any two-dimensional plane of the model parameters when explaining the Higgs data.

(4) The nonobservation of additional Higgs bosons: We employ HiggsBounds-4.3.1 [42,43] to implement the exclusion constraints from the neutral and charged Higgs searches at LEP at the 95% confidence level.

At the LHC run I and run II, the ATLAS and CMS collaborations have searched for the additional scalar state from its decay into various SM channels and some exotic decays. For $gg \to A$ production in the 2HDM of type II, there are destructive interference contributions from the b-quark loop and top-quark loop. The cross section decreases as $\tan\beta$ increases, reaches a minimum value for a moderate value of $\tan\beta$, and is dominated by the b-quark loop for a large enough value of $\tan\beta$. For $gg \to H$ production, the cross section depends on $\sin(\beta-\alpha)$ in addition to $\tan\beta$ and m_H. We compute the cross sections for H and A in gluon fusion and $b\bar{b}$-associated production at next-to-next-to-leading order in QCD via SusHi [44]. The production cross sections of H in the vector-boson fusion process are taken from results of the LHC Higgs Cross Section Working Group [45]. The 2HDMC is used to calculate the branching ratios of the various decay modes of H and A. A complete list of the additional Higgs searches we consider is shown in Table I, where most of channels are taken from Ref. [46]. For $1 \leq \tan\beta \leq 30$, the LHC searches for the heavy charged scalar cannot provide constraints for the model for $m_{H^\pm} > 500$ GeV [29]. Therefore, we do not include the searches for the heavy charged Higgs. In addition, CMS reported the limits on the $hh \to b\bar{b}b\bar{b}$ channel with 2.3 fb^{-1} of data at the 13 TeV LHC [47]. Compared to the corresponding ATLAS channel in Table I [48], the constraints of the $hh \to b\bar{b}b\bar{b}$ channel from CMS are relatively weak due to the low integrated luminosity. Therefore, we do not consider the channel in our analysis.

IV. RESULTS AND DISCUSSIONS

A. Constraints from the 125 GeV Higgs signal data and oblique parameters

The couplings of the SM-like Higgs are sensitive to $\sin(\beta-\alpha)$ and $\tan\beta$. Therefore, the signal data of the 125 GeV Higgs can give strong constraints on the two parameters. In Fig. 1, we show $\sin(\beta-\alpha)$ and $\tan\beta$ allowed

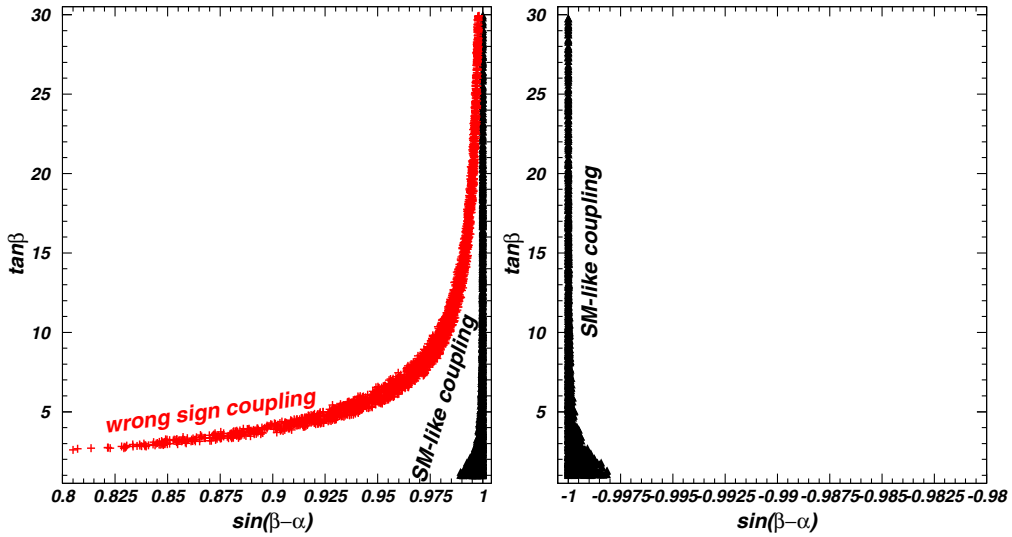

FIG. 1. The samples surviving from the constraints of the 125 GeV Higgs signal data projected onto the plane of $\sin(\beta-\alpha)$ versus $\tan\beta$.

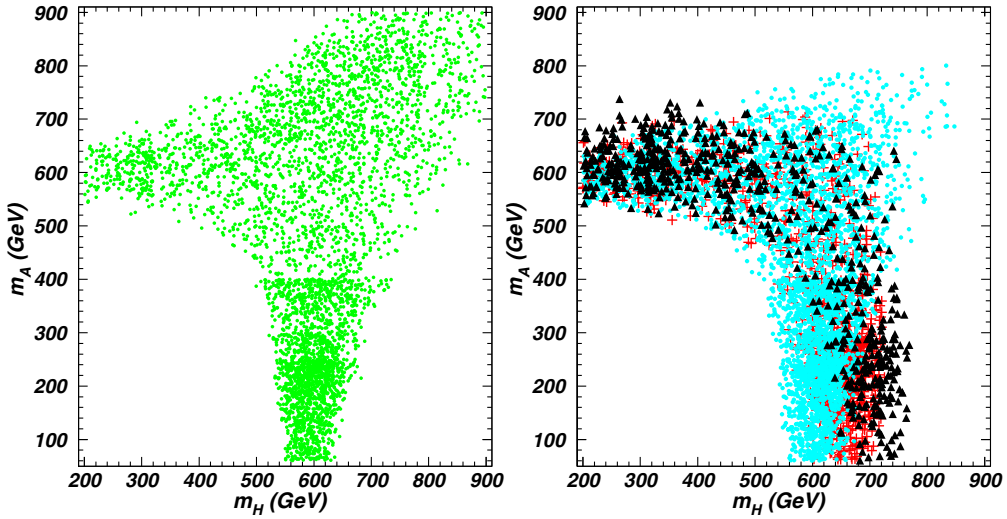

FIG. 2. The surviving samples projected onto the plane of m_H versus m_A under the constraints of vacuum stability, unitarity, perturbativity, and oblique parameters. Left panel: $0.99 \leq |\sin(\beta-\alpha)| \leq 1$ for all of the samples. Right panel: $0.95 \leq \sin(\beta-\alpha) \leq 0.99$ for the bullets (sky blue), $0.90 \leq \sin(\beta-\alpha) \leq 0.95$ for the pluses (red), and $0.80 \leq \sin(\beta-\alpha) \leq 0.90$ for the triangles (black).

by the signal data of the 125 GeV Higgs. From Fig. 1, we find that in the SM-like coupling region of the 125 GeV Higgs, $|\sin(\beta-\alpha)|$ is required to be within the very narrow range $|\sin(\beta-\alpha)| > 0.99$. However, in the wrong-sign Yukawa coupling region of the 125 GeV Higgs, $\sin(\beta-\alpha)$ is allowed to be much smaller than 1, and is always positive. A lower bound is imposed on $\tan\beta$ for a given value of $\sin(\beta-\alpha)$ in the wrong-sign Yukawa coupling region, such as $\tan\beta > 3$ (7) for $\sin(\beta-\alpha) = 0.87(0.97)$, while $\tan\beta$ is allowed to be as low as 1 for any value of $\sin(\beta-\alpha)$ in the SM-like Higgs coupling region.

The oblique parameters S, T, and U can impose strong constraints on the mass spectrum of Higgs bosons in the 2HDM. In Fig. 2, we show m_H and m_A allowed by the constraints of theory and the oblique parameters. The other relevant free parameters are scanned in the following ranges:

$$\begin{aligned} 0.8 \leq |\sin(\beta-\alpha)| \leq 1, \\ 1 \leq \tan\beta \leq 30, \\ 570\ \text{GeV} \leq m_{H^\pm} \leq 900\ \text{GeV}, \\ -(3000\ \text{GeV})^2 \leq m_{12}^2 \leq (3000\ \text{GeV})^2. \end{aligned} \tag{10}$$

Here we use the conventions [36] $0 \leq \beta \leq \frac{\pi}{2}$ and $-\frac{\pi}{2} \leq \beta-\alpha \leq \frac{\pi}{2}$, which leads to $0 \leq \cos(\beta-\alpha) \leq 1$ and $-1 \leq \sin(\beta-\alpha) \leq 1$.

Figure 2 shows that at least one of A and H is required to have a large mass. It is disfavored that both m_A and m_H are smaller than 440 GeV. A light A (H) favors m_H (m_A) to be around 600 GeV for $0.99 < |\sin(\beta-\alpha)| < 1$. With the decreasing of $|\sin(\beta-\alpha)|$, a light A favors an increasing m_H. For example, for $0.8 < \sin(\beta-\alpha) < 0.9$, a light A favors m_H to be around 700 GeV. Note that we do not impose the constraints of the 125 GeV Higgs signal data on the surviving samples in Fig. 2, and therefore cannot determine which samples belong to the SM-like coupling case and which samples belong to the wrong-sign Yukawa coupling case in Fig. 2. However, when combined with Fig. 1, we can deduce that most samples in the right panel of Fig. 2 are disfavored by the SM-like Yukawa coupling of the 125 GeV Higgs.

Now we carve out the allowed parameter space after imposing the joint constraints from theory, precision electroweak data, flavor observables, the 125 GeV Higgs signal data, and especially for the searches for the additional Higgses at the LHC run I and run II. The free parameters $\sin(\beta-\alpha)$, $\tan\beta$, m_{12}^2, and $m_{H^\pm}$ are scanned in the ranges shown in Eq. (10). In order to conveniently show the dependence of m_A (m_H) on the other parameters, we do not scan m_A and m_H simultaneously. Therefore, in each analysis we will fix either m_A or m_H, and perform a detailed examination of the constraints of the Higgs searches on another Higgs. In light of the allowed Higgs mass spectrum shown in Fig. 2, we take four cases: (B1) $m_H = 600$ GeV, (B2) $m_H = 700$ GeV, (C1) $m_A = 600$ GeV, and (C2) $m_A = 700$ GeV. For the four cases another Higgs is allowed to have a wide mass range including the low mass. Since a heavy Higgs can easily avoid the constraints of the Higgs searches, the light Higgs is more interesting.

B. Constraints on the *CP*-odd Higgs

In Fig. 3, fixing $m_H = 600$ GeV and $m_H = 700$ GeV, we project the surviving samples of the SM-like coupling region on the planes of m_A versus $\tan\beta$ and m_A versus $\sin(\beta-\alpha)$ after imposing the pre-LHC constraints (denoting theoretical constraints, electroweak precision data, the flavor observables, R_b, and the exclusion limits from

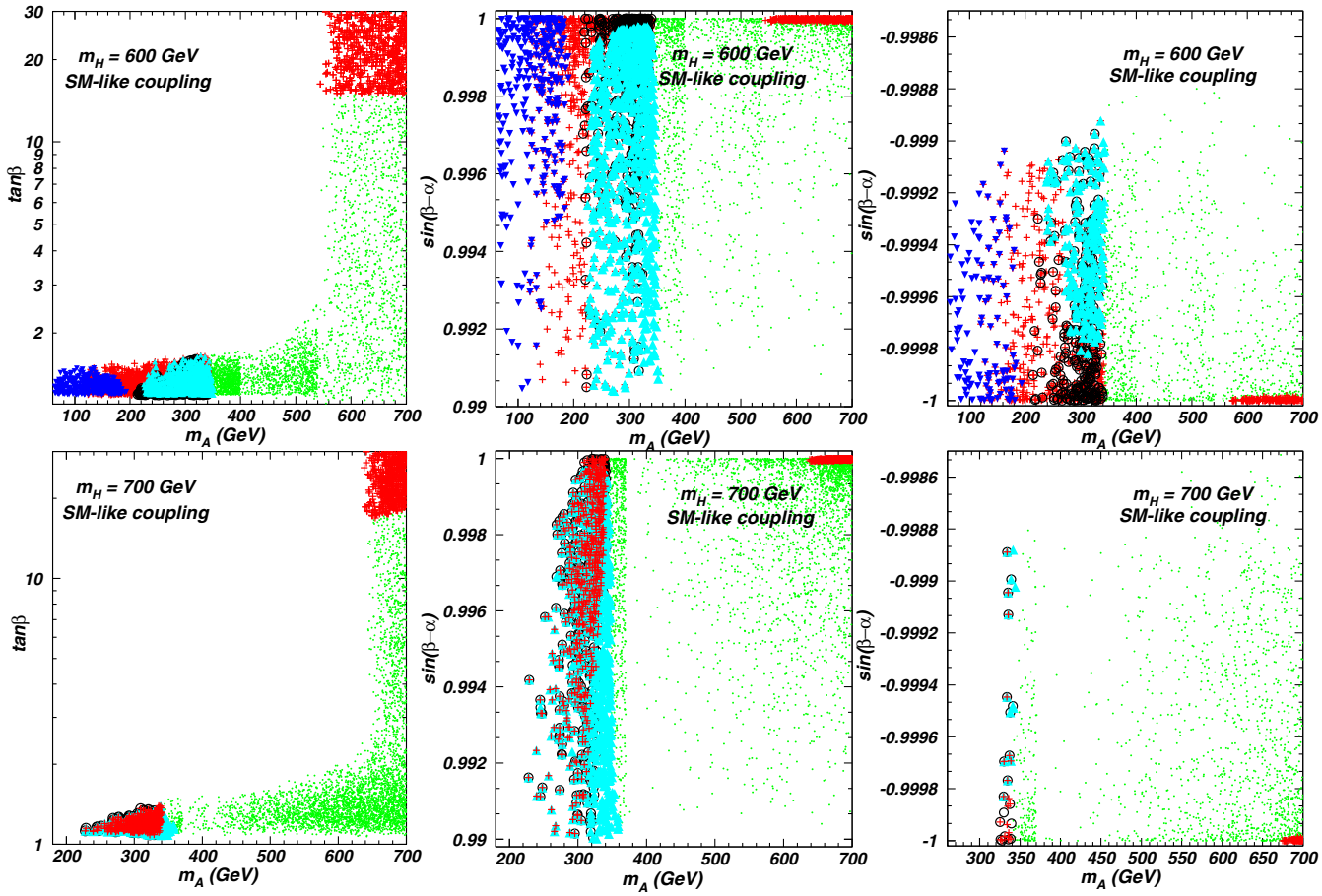

FIG. 3. The surviving samples of the SM-like coupling region projected onto the planes of m_A versus $\tan\beta$ and m_A versus $\sin(\beta-\alpha)$. All of the samples are allowed by pre-LHC constraints (denoting theoretical constraints, electroweak precision data, the flavor observables, R_b, and the exclusion limits from searches for the Higgs at LEP) and the 125 GeV Higgs signal data. The pluses (red), circles (black), triangles (sky blue), and inverted triangles (royal blue) are, respectively, excluded by the $A/H \to \tau^+\tau^-$, $A \to \gamma\gamma$, $A \to hZ$, and $A \to HZ$ searches at the LHC run I and run II.

searches for Higgs at LEP), the 125 GeV Higgs signal data, and the searches for additional Higgses at the LHC run I and run II. The upper-left panel shows that the pre-LHC constraints and the 125 GeV Higgs data give strong constraints on $\tan\beta$ and m_A. $\tan\beta$ is required to be smaller than 2 for $m_A < 500$ GeV and $m_H = 600$ GeV. Further, the $A \to \tau^+\tau^-$, $A \to \gamma\gamma$, $A \to hZ$, and $H \to AZ$ channels exclude the samples in the region of $m_A < 350$ GeV. In the SM-like Higgs coupling region, the coupling constant of $Hb\bar{b}$ is nearly the same as that of $Ab\bar{b}$, and their values are both proportional to $\tan\beta$. The $b\bar{b} \to A/H \to \tau^+\tau^-$ channel can give the upper limit on $\tan\beta$, $\tan\beta < 15$ for m_A $(m_H) < 600$ GeV. With the increasing of m_A, the constraints from the $b\bar{b} \to A \to \tau^+\tau^-$ channel can be weakened, and thus the upper limit of $\tan\beta$ can be larger than 15 for $m_A > 600$ GeV. However, in our analysis we fix $m_H = 600$ GeV which can lead to $\tan\beta < 15$ due to the constraints of the $b\bar{b} \to H \to \tau^+\tau^-$ channel. Therefore, as long as m_H is fixed as 600 GeV, the upper limit of $\tan\beta$ is still 15 with the increasing of m_A.

The upper-middle and upper-right panels show that the $H \to AZ, A \to \gamma\gamma, A \to hZ$ and $A \to \tau^+\tau^-$ channels can give strong constraints on m_A in the case of the approximate alignment limit. With the increasing of $|\sin(\beta-\alpha)|$, the widths of $H \to AZ$ and $A \to hZ$ increase and decrease, respectively. The constraints from the $H \to AZ$ channel become strong as $|\sin(\beta-\alpha)|$ approaches 1, and can exclude most of the samples in the range $m_A < 200$ GeV. The $A \to hZ$ channel can exclude most of samples in the range 220 GeV $< m_A <$ 350 GeV except for the samples that are very close to the alignment limit. For 350 GeV $< m_A <$ 540 GeV, the $A \to t\bar{t}$ channel can sizably enhance the total width of A, and therefore the constraints of the $H \to AZ$, $A \to \gamma\gamma$, and $A \to hZ$ channels can be satisfied. For 540 GeV $< m_A <$ 600 GeV, some samples that are very close to the alignment limit can be excluded by the $b\bar{b} \to A/H \to \tau^+\tau^-$ channel (also see the upper-left panel).

For $m_H = 700$ GeV, the pre-LHC constraints and the 125 GeV Higgs data require m_A to be larger than 220 GeV, and $\tan\beta$ to be smaller than 2 for $m_A < 640$ GeV. In such a

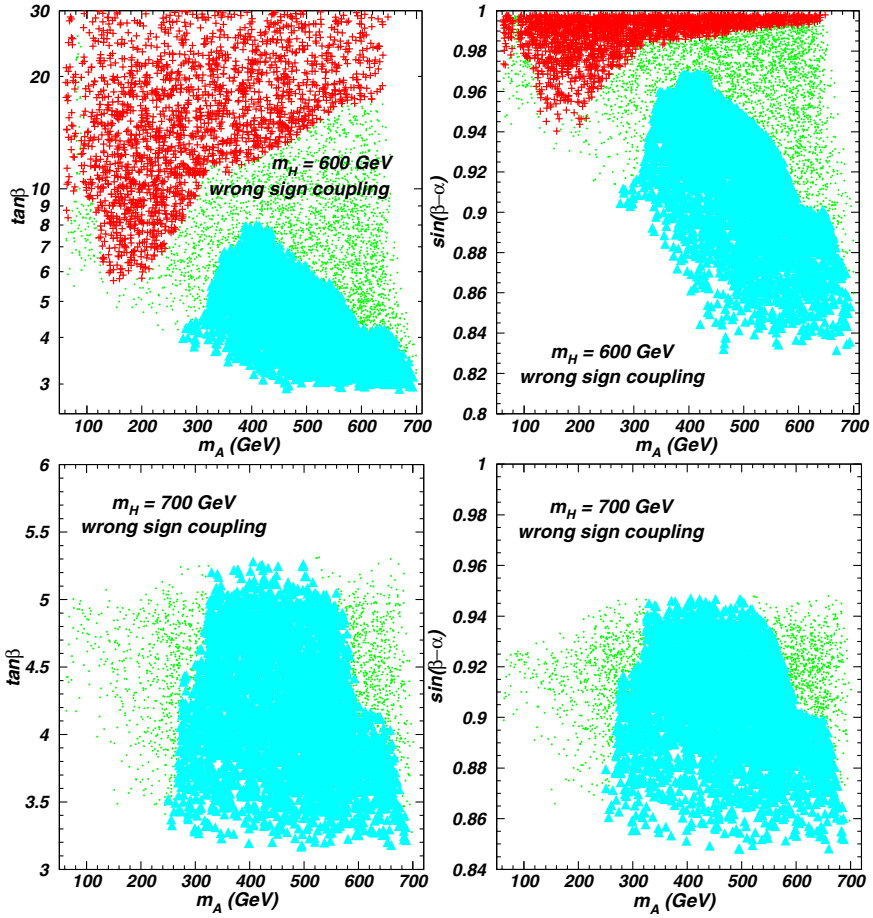

FIG. 4. The surviving samples of the wrong-sign Yukawa coupling region projected onto the planes of m_A versus $\tan\beta$ and m_A versus $\sin(\beta-\alpha)$. All of the samples are allowed by the pre-LHC constraints and the 125 GeV Higgs signal data. The pluses (red) and triangles (sky blue) are, respectively, excluded by the $A/H \to \tau^+\tau^-$ and $A \to hZ$ searches at the LHC run I and run II.

range, all of the samples are allowed by the constraints of the $H \to AZ$ channel. The $A \to \tau^+\tau^-$, $A \to hZ$, and $A \to \gamma\gamma$ channels can exclude $m_A < 340$ GeV. 350 GeV $< m_A <$ 640 GeV is allowed by the pre-LHC constraints, the 125 GeV Higgs data, and the Higgs searches at the LHC. For 640 GeV $< m_A <$ 700 GeV, the $b\bar{b} \to A \to \tau^+\tau^-$ channel can exclude the exact alignment limit and require $\tan\beta$ to be smaller than 18.

Now we examine the parameter space in the wrong-sign Yukawa coupling region for $m_H = 600$ GeV and $m_H =$ 700 GeV. In Fig. 4, we project the surviving samples onto the planes of m_A versus $\tan\beta$ and m_A versus $\sin(\beta-\alpha)$ after imposing the pre-LHC constraints, the 125 GeV Higgs signal data, and the searches for additional Higgses at the LHC run I and run II. In the wrong-sign Yukawa coupling region, the pre-LHC constraints and the 125 GeV Higgs signal data require approximately $\tan\beta > 3$. For such a range of $\tan\beta$, all of the samples are allowed by the $A \to \gamma\gamma$ and $A \to HZ$ channels.

For $m_H = 600$ GeV and 280 GeV $< m_A <$ 700 GeV, the $b\bar{b} \to A \to \tau^+\tau^-$ channel can impose the upper bounds on $\tan\beta$ and $\sin(\beta-\alpha)$, and the $A \to hZ$ channel can impose the lower bounds on $\tan\beta$ and $\sin(\beta-\alpha)$. For example, $4.5 < \tan\beta < 9.0$ and $0.91 < \sin(\beta-\alpha) < 0.975$ for $m_A = 300$ GeV, $8.0 < \tan\beta < 15.0$ and $0.97 < \sin(\beta-\alpha) < 0.99$ for $m_A = 400$ GeV, and $4.0 < \tan\beta < 17.0$ and $0.9 < \sin(\beta-\alpha) < 0.99$ for $m_A = 600$ GeV. The $b\bar{b} \to A \to \tau^+\tau^-$ channel can exclude most of the samples in the range $m_A < 200$ GeV except for a very narrow band of m_A around 100 GeV.

For $m_H = 700$ GeV, the pre-LHC constraints and the 125 GeV Higgs signal data require $\tan\beta < 5.5$ and $\sin(\beta-\alpha) < 0.95$. In such a range, all of the samples are allowed by the constraints of the $b\bar{b} \to A \to \tau^+\tau^-$ channel. The $A \to hZ$ channel can exclude most of the samples in the range 300 GeV $< m_A <$ 600 GeV.

C. Constraints on the heavy *CP*-even Higgs

Here we examine the status of the heavy CP-even Higgs after imposing the relevant theoretical and experimental constraints. In Fig. 5, fixing $m_A = 600$ GeV and $m_A = 700$ GeV, we project the surviving samples onto the planes of m_H versus $\tan\beta$ and m_H versus $\sin(\beta-\alpha)$.

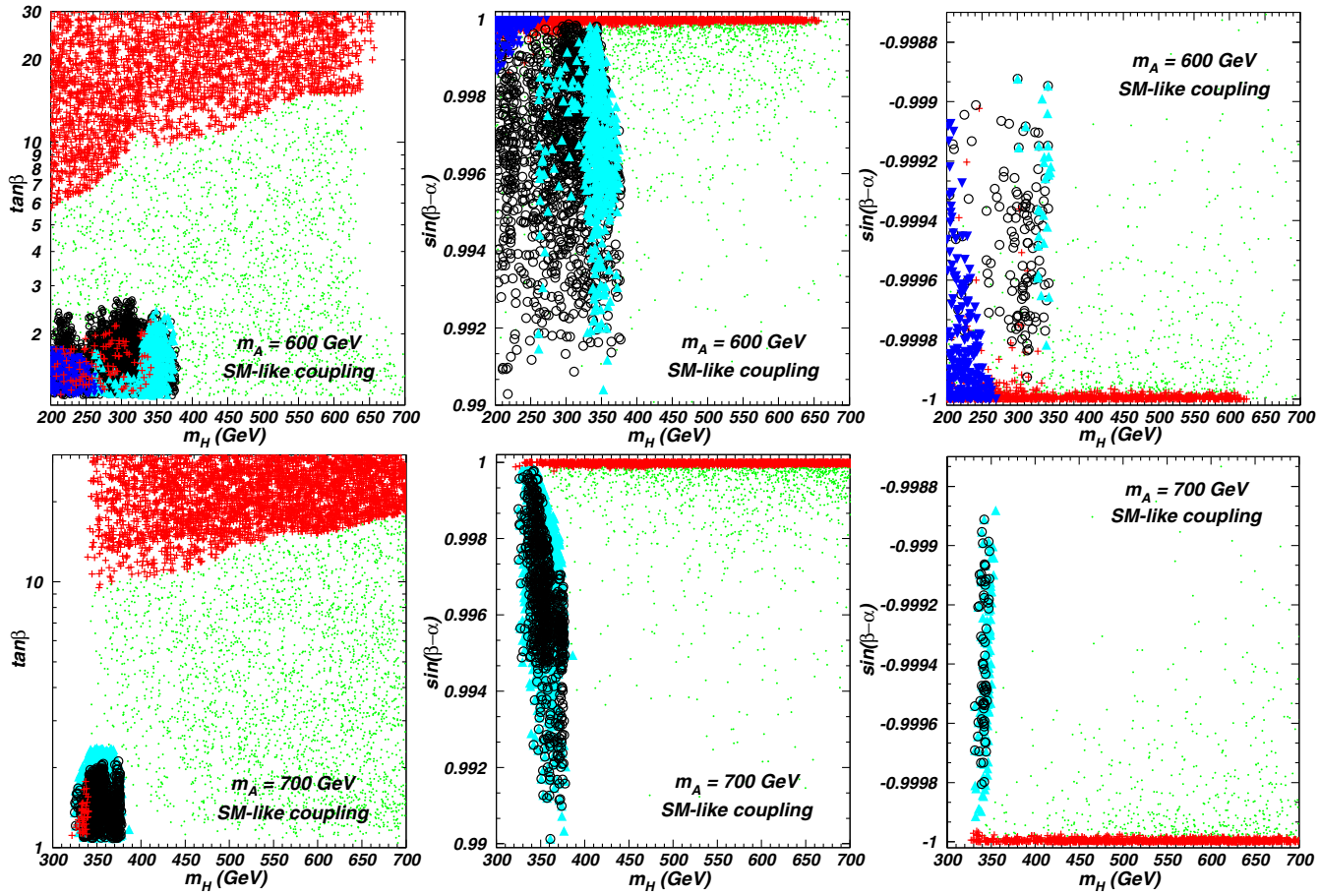

FIG. 5. The surviving samples of the SM-like coupling region projected onto the planes of m_H versus $\tan\beta$ and m_H versus $\sin(\beta-\alpha)$. All the samples are allowed by the pre-LHC constraints and the 125 GeV Higgs signal data. The pluses (red), circles (black), triangles (sky blue), and inverted triangles (royal blue) are, respectively, excluded by the $H/A \to \tau^+\tau^-$, $H \to WW, ZZ, \gamma\gamma$, $H \to hh$, and $A \to HZ$ searches at the LHC run I and run II.

For $m_A = 600$ GeV, the upper-left panel shows that the $b\bar{b} \to H/A \to \tau^+\tau^-$ channel can give the upper bound on $\tan\beta$, such as $\tan\beta < 6$, 10, and 15 for $m_H = 200$, 320, and 600 GeV. The $H \to \tau^+\tau^-$, VV, $\gamma\gamma$, hh and $A \to HZ$ searches can require $\tan\beta > 2.5$ for $m_H < 380$ GeV. The appropriate values of $\tan\beta$ can simultaneously suppress the cross sections of the Higgs in gluon-fusion production and $b\bar{b}$-quark associated production. In addition, the $H \to b\bar{b}$ channel can be the dominant decay mode, so that the branching ratios of $H \to VV$, $\gamma\gamma$, and hh will be sizably suppressed, and the constraints from these channels can be avoided.

For $m_A = 600$ GeV, the upper-middle and upper-right panels of Fig. 5 show that for the proper $\tan\beta$ (see the upper-left panel), the $H/A \to \tau^+\tau^-$, $H \to VV$, $\gamma\gamma$, hh, and $A \to HZ$ channels can give strong constraints on m_H when close to the alignment limit. All of the samples in the range $m_H > 270$ GeV can satisfy the constraints of the $A \to HZ$ channel. The widths of $H \to VV$, hh decrease with the increasing of $|\sin(\beta-\alpha)|$ and are equal to zero in the exact-alignment limit. In the proper deviation from the alignment limit, the searches for these channels can exclude most of the samples in the range $m_H < 380$ GeV. With the increasing of m_H, the $H \to t\bar{t}$ channel can enhance the total width of H sizably, so that the constraints from the $H \to VV$, $\gamma\gamma$, and hh channels can be relaxed. Note that in the upper-middle and upper-right panels of Fig. 5, there are some allowed points mixed among the excluded points. These allowed points have appropriate values of $\tan\beta$, as shown in the upper-left panel of Fig. 5.

For $m_A = 700$ GeV, the lower-left panel of Fig. 5 shows that the pre-LHC constraints and the 125 GeV Higgs signal data require $m_H > 300$ GeV. In such a range, all of the samples are allowed by the constraints of the $A \to HZ$ channel. The other features of the parameter space are similar to those of $m_A = 600$ GeV.

Now we examine the parameter space in the wrong-sign Yukawa coupling region for $m_A = 600$ GeV and $m_A = 700$ GeV. In Fig. 6, we project the surviving samples onto the planes of m_H versus $\tan\beta$ and m_H versus $\sin(\beta-\alpha)$ after imposing the pre-LHC constraints, the 125 GeV Higgs signal data, and the searches for additional Higgses at the

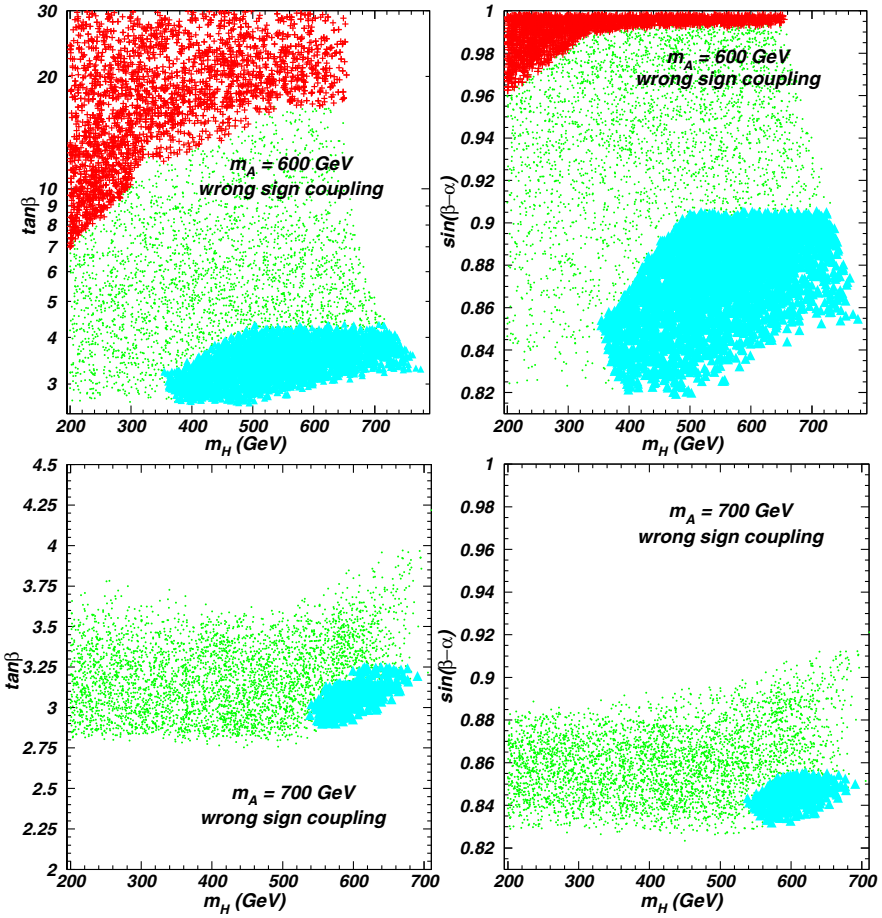

FIG. 6. The surviving samples of the wrong-sign Yukawa coupling region projected onto the planes of m_H versus $\tan\beta$ and m_H versus $\sin(\beta-\alpha)$. All of the samples are allowed by the pre-LHC constraints and the 125 GeV Higgs signal data. The pluses (red) and triangles (sky blue) are, respectively, excluded by the $H/A \to \tau^+\tau^-$ and $A \to hZ$ searches at the LHC run I and run II.

LHC run I and run II. The pre-LHC constraints and the 125 GeV Higgs signal data require $\tan\beta$ to be much larger than 2 in the wrong-sign Yukawa coupling region. For such a range of $\tan\beta$, all of the samples are allowed by the constraints of the $H \to VV$, $\gamma\gamma$, hh, and $A \to HZ$ channels.

For $m_A = 600$ GeV, the $b\bar{b} \to H \to \tau^+\tau^-$ channel can impose the upper bounds on $\tan\beta$ and $\sin(\beta-\alpha)$. For

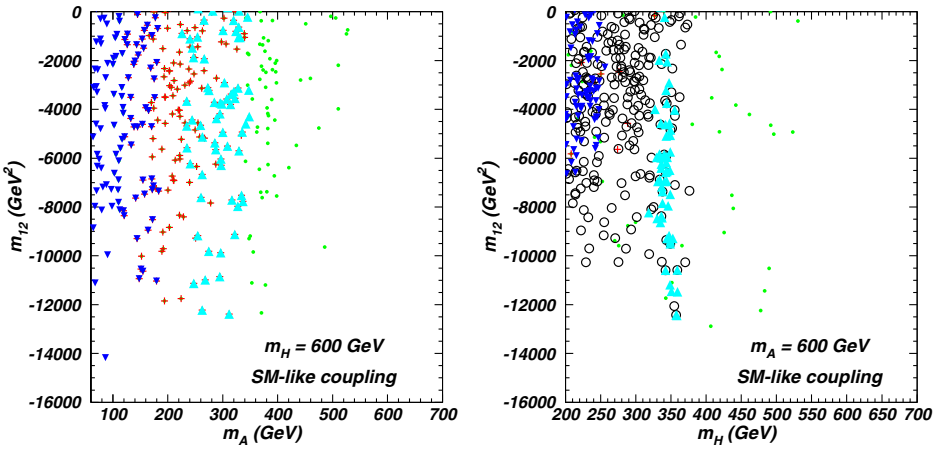

FIG. 7. The surviving samples with negative values of m_{12}^2 projected onto the planes of m_A versus m_{12}^2 and m_H versus m_{12}^2. The meanings of the symbols in the left (right) panel are the same as in Fig. 3 (Fig. 5).

example, $\tan\beta < 7.0$ and $\sin(\beta-\alpha) < 0.96$ for $m_H = 200$ GeV, $\tan\beta < 10.0$ and $\sin(\beta-\alpha) < 0.98$ for $m_H = 300$ GeV, and $\tan\beta < 16.0$ and $\sin(\beta-\alpha) < 0.99$ for $m_H = 600$ GeV. All of the samples in the range $m_H < 350$ GeV can survive from the constraints of the $A \to hZ$ channel. In such a range of m_H, the $A \to HZ$ mode can enhance the total width of A, and lead to a suppression of the branching ratio of $A \to hZ$. For $m_H > 350$ GeV, the $A \to hZ$ channel can exclude most of the samples in the range $\tan\beta < 4.5$ and $\sin(\beta-\alpha) < 0.905$.

For $m_A = 700$ GeV, the pre-LHC constraints and the 125 GeV Higgs signal data require $\tan\beta < 4$ and $\sin(\beta-\alpha) < 0.92$. In such a range, all of the samples are allowed by the constraints of the $b\bar{b} \to H \to \tau^+\tau^-$ channel. The $A \to hZ$ channel can exclude most of the samples in the ranges of $m_H > 540$ GeV, $\tan\beta < 3.25$, and $\sin(\beta-\alpha) < 0.855$.

Negative values of m_{12}^2 may lead to a situation where the SM vacuum is a metastable vacuum with a deeper vacuum lying somewhere else, a situation denoted as a panic vacuum in Ref. [72]. We find that some negative values of m_{12}^2 are allowed in the SM-like coupling region of the 125 GeV Higgs for the cases of $m_H = 600$ GeV or $m_A = 600$ GeV, and the negative m_{12}^2 is excluded in the other cases taken in this paper. In Fig. 7, we show the allowed negative values of m_{12}^2 in our scans.

V. CONCLUSION

We examined the parameter space of the 2HDM of type II after imposing the relevant theoretical and experimental constraints from precision electroweak data, B-meson decays, R_b, the 125 GeV Higgs signal data, and the $H/A \to \tau^+\tau^-$, $\gamma\gamma$, $H \to WW$, ZZ, hh, AZ, and $A \to hZ$, HZ searches at the LHC run I and run II. We have obtained the following results.

(i) Status of the CP-odd Higgs A: Due to the constraints from theory and the oblique parameters, for m_H around 600–700 GeV, the CP-odd Higgs A is allowed to have a wide mass range, including the low mass. In the SM-like Higgs coupling region of the 125 GeV Higgs, the $A \to hZ$, $\gamma\gamma$, $\tau^+\tau^-$ channels can exclude 140 GeV $< m_A <$ 350 GeV. For $m_H = 600$ GeV, the $H \to AZ$ channel can exclude most of the samples in the range $m_A < 200$ GeV. The $b\bar{b} \to A/H \to \tau^+\tau^-$ channel can impose the upper limits on $\tan\beta$ and $|\sin(\beta-\alpha)|$ in the large mass range. The parameter spaces of $\tan\beta < 2$, $0.99 \le \sin(\beta-\alpha) \le 1$, and $-1 \le \sin(\beta-\alpha) \le -0.998$ are allowed for $m_H = 600$ GeV and 350 GeV $< m_A <$ 540 GeV as well as $m_H = 700$ GeV and 350 GeV $< m_A <$ 640 GeV.

In the wrong-sign Yukawa coupling region of the 125 GeV Higgs, for $m_H = 600$ GeV and 280 GeV $< m_A <$ 700 GeV, the $b\bar{b} \to A \to \tau^+\tau^-$ channel can impose the upper bounds on $\tan\beta$ and $\sin(\beta-\alpha)$, and the $A \to hZ$ channel can impose the lower bounds on $\tan\beta$ and $\sin(\beta-\alpha)$. The $b\bar{b} \to A \to \tau^+\tau^-$ channel can exclude most of the samples in the range $m_A < 200$ GeV except for a very narrow band of m_A around 100 GeV. Compared to the case of $m_H = 600$ GeV, for the case of $m_H = 700$ GeV, 320 GeV $< m_A <$ 500 GeV is excluded, and the allowed parameter space is narrowed since pre-LHC constraints and the 125 GeV Higgs signal data require $\tan\beta < 5.5$ and $\sin(\beta-\alpha) < 0.95$.

(ii) Status of the heavy CP-even Higgs H: For m_A around 600 GeV, the CP-even Higgs H is allowed to have a wide mass range. In the SM-like Higgs coupling region of the 125 GeV Higgs, the $b\bar{b} \to H/A \to \tau^+\tau^-$ channels give the upper bound on $\tan\beta$, such as $\tan\beta < 6$, 10, and 15 for $m_H = 200$, 320, and 600 GeV, respectively. The $H \to \tau^+\tau^-$, WW, ZZ, $\gamma\gamma$, hh channels require $\tan\beta > 2.5$ for $m_H < 380$ GeV. For $m_A = 600$ GeV, the $A \to HZ$ channel can exclude most of the samples in the range $m_H < 270$ GeV. For the proper $\tan\beta$ and $\sin(\beta-\alpha)$, m_H is allowed to be as low as 200 GeV for $m_A = 600$ GeV, and 300 GeV for $m_A = 700$ GeV.

In the wrong-sign Yukawa coupling region of the 125 GeV Higgs, the $b\bar{b} \to H \to \tau^+\tau^-$ channel can impose the upper bounds on $\tan\beta$ and $\sin(\beta-\alpha)$. For $m_A = 600$ GeV, the $A \to hZ$ channel can exclude most of the samples in the ranges $\tan\beta < 4.5$, $\sin(\beta-\alpha) < 0.905$, and $m_H > 350$ GeV. Compared to the case of $m_A = 600$ GeV, for the case of $m_A = 700$ GeV, the allowed parameter space is narrowed since pre-LHC constraints and the 125 GeV Higgs signal data require $\tan\beta < 4$ and $\sin(\beta-\alpha) < 0.92$. For the proper $\tan\beta$ and $\sin(\beta-\alpha)$, m_H is allowed to be as low as 200 GeV for both $m_A = 600$ GeV and $m_A = 700$ GeV.

ACKNOWLEDGMENTS

We thank Qing-Hong Cao, Ye Chen, and Weimin Song for helpful discussions. This work is supported by the National Natural Science Foundation of China under Grant No. 11575152.

[1] S. Chatrchyan *et al.* (CMS Collaboration), Phys. Lett. B **716**, 30 (2012).
[2] G. Aad *et al.* (ATLAS Collaboration), Phys. Lett. B **716**, 1 (2012).
[3] ATLAS and CMS Collaborations, J. High Energy Phys. 08 (2016) 045.
[4] T. D. Lee, Phys. Rev. D **8**, 1226 (1973).
[5] H. E. Haber, G. L. Kane, and T. Sterling, Nucl. Phys. **B161**, 493 (1979).
[6] L. J. Hall and M. B. Wise, Nucl. Phys. **B187**, 397 (1981).
[7] J. F. Donoghue and L. F. Li, Phys. Rev. D **19**, 945 (1979).
[8] V. D. Barger, J. L. Hewett, and R. J. N. Phillips, Phys. Rev. D **41**, 3421 (1990).
[9] Y. Grossman, Nucl. Phys. **B426**, 355 (1994).
[10] A. G. Akeroyd and W. J. Stirling, Nucl. Phys. **B447**, 3 (1995).
[11] A. G. Akeroyd, Phys. Lett. B **377**, 95 (1996).
[12] A. Celis, V. Ilisie, and A. Pich, J. High Energy Phys. 07 (2013) 053.
[13] B. Grinstein and P. Uttayarat, J. High Energy Phys. 06 (2013) 094; 09 (2013) 110(E).
[14] C.-Y. Chen, S. Dawson, and M. Sher, Phys. Rev. D **88**, 015018 (2013).
[15] N. Craig, J. Galloway, and S. Thomas, arXiv:1305.2424.
[16] O. Eberhardt, U. Nierste, and M. Wiebusch, J. High Energy Phys. 07 (2013) 118.
[17] B. Dumont, J. F. Gunion, Y. Jiang, and S. Kraml, Phys. Rev. D **90**, 035021 (2014).
[18] E. J. Chun, Z. Kang, M. Takeuchi, and Y.-L. S. Tsai, J. High Energy Phys. 11 (2015) 099.
[19] S.-H. Zhu, Nucl. Part. Phys. Proc. **273–275**, 716 (2016).
[20] D. Chowdhury and O. Eberhardt, J. High Energy Phys. 11 (2015) 052.
[21] V. Cacchio, D. Chowdhury, O. Eberhardt, and C. W. Murphy, J. High Energy Phys. 11 (2016) 026.
[22] N. Chakrabarty, U. K. Dey, and B. Mukhopadhyaya, J. High Energy Phys. 12 (2014) 166.
[23] J. Baglio, O. Eberhardt, U. Nierste, and M. Wiebusch, Phys. Rev. D **90**, 015008 (2014).
[24] J. Bernon, B. Dumont, and S. Kraml, Phys. Rev. D **90**, 071301 (2014).
[25] N. Craig, F. DEramo, P. Draper, S. Thomas, and H. Zhang, J. High Energy Phys. 06 (2015) 137.
[26] J. Bernon, J. F. Gunion, H. E. Haber, Y. Jiang, and S. Kraml, Phys. Rev. D **92**, 075004 (2015).
[27] F. Kling, A. Pyarelal, and S. Su, J. High Energy Phys. 11 (2015) 051.
[28] A. G. Akeroyd *et al.*, Eur. Phys. J. C **77**, 276 (2017).
[29] S. Moretti, arXiv:1612.02063.
[30] G. C. Dorsch, S. J. Huber, K. Mimasu, and J. M. No, Phys. Rev. D **93**, 115033 (2016).
[31] F. Kling, J. M. No, and S. Su, J. High Energy Phys. 09 (2016) 093.
[32] V. Khachatryan *et al.* (CMS Collaboration), Report No. CMS-PAS-HIG-14-029.
[33] R. A. Battye, G. D. Brawn, and A. Pilaftsis, J. High Energy Phys. 08 (2011) 020.
[34] P. S. Bhupal Dev and A. Pilaftsis, J. High Energy Phys. 12 (2014) 024.
[35] Y. Amhis *et al.* (Heavy Flavor Averaging Group), arXiv:1612.07233; M. Misiak and M. Steinhauser, Eur. Phys. J. C **77**, 201 (2017).
[36] D. Eriksson, J. Rathsman, and O. Stål, Comput. Phys. Commun. **181**, 189 (2010).
[37] D. Eriksson, J. Rathsman, and O. Stål, Comput. Phys. Commun. **181**, 833 (2010).
[38] F. Mahmoudi, Comput. Phys. Commun. **180**, 1579 (2009).
[39] C. Q. Geng and J. N. Ng, Phys. Rev. D **38**, 2857 (1988); **41**, 1715(E) (1990).
[40] H. E. Haber and H. E. Logan, Phys. Rev. D **62**, 015011 (2000).
[41] G. Degrassi and P. Slavich, Phys. Rev. D **81**, 075001 (2010).
[42] P. Bechtle, O. Brein, S. Heinemeyer, G. Weiglein, and K. E. Williams, Comput. Phys. Commun. **181**, 138 (2010).
[43] P. Bechtle, O. Brein, S. Heinemeyer, O. Stål, T. Stefaniak, G. Weiglein, and K. E. Williams, Eur. Phys. J. C **74**, 2693 (2014).
[44] R. V. Harlander, S. Liebler, and H. Mantler, Comput. Phys. Commun. **184**, 1605 (2013).
[45] S. Heinemeyer *et al.* (LHC Higgs Cross Section Working Group), arXiv:1307.1347.
[46] R. K. Barman, B. Bhattacherjee, A. Choudhury, D. Chowdhury, J. Lahiri, and S. Ray, arXiv:1608.02573.
[47] V. Khachatryan *et al.* (CMS Collaboration), Report No. CMS-PAS-HIG-16-002.
[48] ATLAS Collaboration, Report No. ATLAS-CONF-2016-049.
[49] G. Aad *et al.* (ATLAS Collaboration), J. High Energy Phys. 11 (2014) 056.
[50] CMS Collaboration, Phys. Lett. B **758**, 296 (2016).
[51] ATLAS Collaboration, Report No. ATLAS-CONF-2016-085.
[52] CMS Collaboration, Report No. CMS-PAS-HIG-16-037.
[53] ATLAS Collaboration, Report No. ATLAS-CONF-2016-059.
[54] CMS Collaboration, Report No. CMS-PAS-EXO-16-027.
[55] G. Aad *et al.* (ATLAS Collaboration), J. High Energy Phys. 01 (2016) 032.
[56] ATLAS Collaboration, Report No. ATLAS-CONF-2016-074.
[57] G. Aad *et al.* (ATLAS Collaboration), Report No. ATLAS-CONF-2016-062.
[58] G. Aad *et al.* (ATLAS Collaboration), Eur. Phys. J. C **76**, 45 (2016).
[59] ATLAS Collaboration, Report No. ATLAS-CONF-2016-056.
[60] ATLAS Collaboration, Report No. ATLAS-CONF-2016-082.
[61] ATLAS Collaboration, Report No. ATLAS-CONF-2016-079.
[62] V. Khachatryan *et al.* (CMS Collaboration), Phys. Rev. D **94**, 052012 (2016).
[63] V. Khachatryan *et al.* (CMS Collaboration), Phys. Lett. B **749**, 560 (2015).
[64] V. Khachatryan *et al.* (CMS Collaboration), Phys. Lett. B **755**, 217 (2016).
[65] ATLAS Collaboration, Report No. ATLAS-CONF-2016-004.

[66] V. Khachatryan *et al.* (CMS Collaboration), Report No. CMS-PAS-HIG-16-032.
[67] CMS Collaboration, Report No. CMS-PAS-HIG-16-029.
[68] V. Khachatryan *et al.* (CMS Collaboration), Phys. Lett. B **748**, 221 (2015).
[69] G. Aad *et al.* (ATLAS Collaboration), Phys. Lett. B **744**, 163 (2015).
[70] ATLAS Collaboration, Report No. ATLAS-CONF-2016-015.
[71] V. Khachatryan *et al.* (CMS Collaboration), Phys. Lett. B **759**, 369 (2016).
[72] A. Barroso, P. M. Ferreira, I. P. Ivanov, and R. Santos, J. High Energy Phys. 06 (2013) 045.